

# Delineating the Clinical Phenotype of Patients With the c.629C>G, p.Pro210Arg Mutation in *Peripherin-2*

Shannon M. Conley,<sup>1</sup> Cynthia K. McClard,<sup>2,3</sup> Maggie L. Mwoyosvi,<sup>1</sup> Niyaf Alkadhem,<sup>2</sup> Bojana Radojevic,<sup>2</sup> Martin Klein,<sup>4</sup> David Birch,<sup>4</sup> Ashley Ellis,<sup>3</sup> Sonny W. Icks,<sup>3</sup> Tejesh Guddanti,<sup>5</sup> and Lea D. Bennett<sup>2,3</sup>

<sup>1</sup>University of Oklahoma Health Sciences Center, Department of Cell Biology, Oklahoma City, Oklahoma, United States

<sup>2</sup>University of Oklahoma Health Sciences Center, Department of Ophthalmology, Oklahoma City, Oklahoma, United States

<sup>3</sup>Dean McGee Eye Institute, Oklahoma City, Oklahoma City, Oklahoma, United States

<sup>4</sup>Retina Foundation of the Southwest, Dallas, Texas, United States

<sup>5</sup>University of Oklahoma Health Sciences Center, College of Medicine, Oklahoma City, Oklahoma, United States

Correspondence: Lea D. Bennett, 608 Stanton L. Young Blvd, Oklahoma City, OK 73104, USA; [lbennett@ouhsc.edu](mailto:lbennett@ouhsc.edu).

Received: February 8, 2022

Accepted: June 29, 2022

Published: July 21, 2022

Citation: Conley SM, McClard CK, Mwoyosvi ML, et al. Delineating the clinical phenotype of patients with the c.629C>G, p.Pro210Arg mutation in *peripherin-2*. *Invest Ophthalmol Vis Sci.* 2022;63(8):19. <https://doi.org/10.1167/iovs.63.8.19>

**PURPOSE.** More than 200 different mutations in peripherin-2 (*PRPH2*) are associated with multiple subtypes of inherited retinal diseases (IRDs), including retinitis pigmentosa and cone or macular diseases. Our goal was to understand how the poorly characterized *PRPH2* mutation p.Pro210Arg (P210R) affects visual function and retinal structure as well as gain insight into the mechanism driving the clinical pathology.

**METHODS.** Eleven patients had clinical assessments including best-corrected visual acuity (BCVA), full field and multifocal electroretinography (ERG), static (spot size V) and kinetic perimetry (Octopus 900), and dark-adapted chromatic (DAC; Medmont; spot size V) perimetry. Images were acquired with the Optos ultra-wide field camera and spectral-domain optical coherence tomography (SD-OCT). Molecular characteristics of the P210R mutant protein were evaluated in vitro.

**RESULTS.** Patients with the P210R mutation had BCVA (Snellen) ranging from 20/15 to 20/80. Perimetry showed a reduction in sensitivity, while ERG findings suggested that cone function was more impaired than rod function. Scotomas were identified corresponding to atrophic retinal lesions. Imaging revealed heterogeneous outer retinal changes such as hyperfluorescent flecks, hypo-autofluorescence (AF) regions of atrophy, and thinning of the photoreceptor layer on SD-OCT. In vitro findings suggested that P210R-Prph2 retains the ability to interact with binding partner Rom1 but abnormally accumulates in the endoplasmic reticulum (ER), suggesting the protein does not fold properly.

**CONCLUSIONS.** Rod and cone sensitivities were decreased in subjects with the P210R mutation in *PRPH2*. There was scotomatous vision loss that occurred within the macula, likely due to atrophy that occurs after drusen have formed and have begun to resolve. This suggests that although rod and cone photoreceptors are dependent on *PRPH2*, preventing blindness in this specific subgroup of patients could involve therapeutics that impede the formation or lifecycle of drusen.

Keywords: inherited retinal disease (IRD), peripherin-2 (*PRPH2*), macular or pattern dystrophy, drusen

Peripherin-2 (*PRPH2*), formerly known as retinal degeneration slow (RDS), is a retina-specific glycoprotein that is essential for photoreceptor disc morphogenesis.<sup>1-4</sup> *PRPH2* co-localizes with its non-glycosylated homologue retinal outer segment membrane protein 1 (*ROM1*) to the rim region of rod outer segment discs and cone lamellae.<sup>5-8</sup> Similar to other members of the tetraspanin protein superfamily, *PRPH2* and *ROM1* contain four transmembrane domains, cytoplasmic N- and C-termini, and a small cytoplasmic loop in addition to two extracellular/intradiscal loops. The large second intradiscal loop (D2) is a key functional domain for *PRPH2/ROM1* oligomerization, and proper fold-

ing of this region requires three intramolecular disulfide bonds mediated by six D2 loop cysteines.<sup>9</sup> *PRPH2* and *ROM1* assemble into hetero-tetramer and -octamer complexes that are held together by noncovalent interactions in the D2 loop.<sup>9-11</sup> Additionally, *PRPH2* forms higher order, covalently linked homo-oligomers, assembled via intermolecular disulfide bonds mediated by a seventh cysteine (C150) in the D2 loop. These homo-oligomers are essential for outer segment disc formation<sup>12</sup>; mice that cannot form covalently-linked complexes (e.g. *Prph2* C150S) develop photoreceptors that initiate disc formation but the outer segments fail to elongate and the retina undergoes rapid degeneration.<sup>5,13,14</sup>

Conversely, mice without *Prph2* expression (*Rds* mice) are completely devoid of outer segments<sup>1</sup> and a slow degeneration of the retina is observed.

Mutations in the *PRPH2* gene have been associated with multiple clinical phenotypes, including pattern dystrophy (PD), cone rod dystrophy (CRD), retinitis pigmentosa (RP), and other chorioretinal or macular dystrophies.<sup>15</sup> Although *PRPH2* disease is generally autosomal dominant (ad), a digenic pattern has been reported in conjunction with specific nonpathogenic variants in *ROM1*.<sup>16,17</sup> A case study of one patient with a retinal disease has been reported to harbor only a *ROM1* mutation.<sup>18</sup> However, this study did not perform family or molecular analysis to confirm that the mutation segregated with disease or that the variant was deleterious to cell function. Without evaluating the noncoding regions as potential sites for mutations or testing the DNA for copy number variants in known inherited retinal disease (IRD) genes, further studies are needed to address the ongoing interest in understanding whether there may be IRDs associated with *ROM1* variants. However, it has been suggested that the presence of *ROM1* variants could modify the clinical presentation<sup>19</sup> or increase the severity of *PRPH2*-related IRD.<sup>20</sup> The *PRPH2* variant c.629C>G (p.Pro210Arg or P210R) is a pathogenic missense mutation that has been reported in 5 studies, with a total of 13 identified individuals harboring this mutation.<sup>21–25</sup> The P210R mutation occurs within the D2 loop domain, quite near to 2 of the cysteines involved in intramolecular disulfide bonds (C213/C214), and thus may affect *PRPH2* protein structure. This hypothesis is supported by evidence from other *PRPH2* disease models showing that introducing mutations at D2 loop cysteines (e.g. C214S, C213Y, and C150S)<sup>13,26–28</sup> or near D2 loop cysteines (e.g. K153del, Y141C)<sup>19,29–31</sup> results in various alterations in *PRPH2*/*ROM1* complex assembly and consequent structural and functional defects in rod and cone photoreceptors.

Research completed in both the clinic and in animal models over the past several decades has highlighted that *PRPH2* phenotypes vary from mutation to mutation, and frequently exhibit significant intrafamilial/within-mutation phenotypic heterogeneity. These studies are complicated by the limited sizes of phenotypically characterized patient cohorts carrying *PRPH2* mutations and the need to make animal models for individual mutations. Here, our goal was to begin to understand the disease mechanisms associated with the *PRPH2* P210R mutation by conducting clinical evaluations of 11 patients combined with in vitro studies to evaluate molecular and cellular consequences of the P210R mutation. To date, this is the first report on the disease mechanism associated with P210R and the largest clinically characterized cohort of unrelated patients with this *PRPH2* mutation.

## MATERIALS AND METHODS

### Patient Population

Informed consent was obtained prior to examinations. The data presented here were retrospective analyses of patients who had been previously determined to harbor the P210R mutation in *PRPH2*. Standard operating procedures were applied for clinical testing that were performed at the Retina Foundation of the Southwest (Dallas, TX, USA) or Dean McGee Eye Institute (Oklahoma City, OK, USA). All proce-

dures were approved by institutional ethics review boards and adhered to the Declaration of Helsinki.

### Clinical Evaluation

The best-corrected visual acuity (BCVA) was measured with the Electronic Visual Acuity Tester (Jaeb Center for Health Research, Tampa, FL, USA). The eye with the lower acuity (or the right eye if acuity was the same) was dilated (tropicamide 1% and phenylephrine 2.5%) and patched for 30 minutes to allow dark adaptation. During dark-adaptation, the better-seeing (or left) eye underwent static and kinetic perimetry (Octopus900; Haag-Streit AG; Koeniz, Switzerland) and the Farnsworth Dichotomous<sup>32</sup> color (Panel D-15) test. The kinetic visual fields were mapped using spot sizes V-4e, III-4e, and I-4e at a speed of 4 degrees /second. Static perimetry was performed on Octopus 900 (Haag Streit, Koeniz, Switzerland) with a 164 point grid by GATE strategy with spot size V or on the Humphrey Field Analyzer (HFA; Carl Zeiss Meditec, Dublin, CA, USA) with standard 30-2 Swedish Interactive Threshold Algorithm (SITA) protocol following standard procedures. Appropriate refraction with additional adjustment for age was provided for each patient when the central visual field was tested. During the perimetry sessions, the non-examined eye of the patient was occluded. The dilated and dark-adapted eye was subjected to dark-adapted chromatic (DAC) perimetry (Medmont International Pty Ltd., Victoria, Australia).<sup>33,34</sup> Immediately after DAC perimetry, full-field electroretinography (ffERG; Espion system; Diagnosis LLC, Lowell, MA, U.S.A.) was performed on the same dark-adapted eye with the International Society for Clinical Electrophysiology of Vision (ISCEV) standard protocol.<sup>35</sup> Multifocal ERG (mfERG) was performed on the Veris (Veris Science 5.1.10x; EDI, San Mateo, CA, USA) under standard ISCEV guidelines.<sup>35</sup> Results from DAC and ffERG testing were compared to normal reference values as previously determined.<sup>34,36</sup> Normal references for the Octopus 900, HFA, and mfERG were included in the software.

After functional testing, retinal imaging was performed. Images were acquired with spectral domain optical coherence tomography (SD-OCT; Spectralis Heidelberg retina angiography + OCT; Heidelberg Engineering, Inc., Heidelberg, Germany). Automatic real-time registration was used with a mean of 100 scans for high-resolution images of both eyes (OU). The SD-OCT camera was used to obtain blue auto-AF (BAF) images of dilated left eyes. For patients D1 and E1, the left eye was dilated after functional testing but before BAF imaging. Wide-field fundus images of dilated left eyes were acquired with the Optos camera (Optos PLC, Dunfermline, UK) to obtain pseudocolored and autofluorescence retinal images. The CF-60UD (Canon USA Inc., Lake Success, NY, USA) was used to collect fundus images. Some data were previously reported for patients A1, A2, and C1. These data are indicated with the reference citation in the tables. Otherwise, the data presented here have not been previously reported.

### Transfection and Plasmids

Plasmid constructs containing a cytomegalovirus (CMV) promoter driving wild type murine (WT) *Prph2*, and *Rom1* cDNA were cloned into the PKH3 vector using standard approaches and were generously shared by Dr. Muna Naash (University of Houston). The P210R mutation was introduced using site-directed mutagenesis and was confirmed

TABLE 1. Primary Antibodies

Antigen	Antibody	Species	Source	Concentration
Prph2	RDS-CT	Rbt-PC	Dr. Muna Naash <sup>12,13</sup>	ICC 1:1,000IP: 1ul/sample
Prph2	mAB RDS2B7	Ms-MC	Dr. Muna Naash <sup>30,61,62</sup>	WB 1:500
Rom1	ROM1-CT	Rbt-PC	Dr. Muna Naash <sup>12,13</sup>	WB 1:1,000
Rom1	mAB 2H5	Ms-MC	Dr. Muna Naash <sup>31,62</sup>	ICC 1:1000
Calreticulin	Calreticulin	Ckn-PC	Abcam (Ab #2908) <sup>19,38</sup>	ICC 1:500

PC, polyclonal; MC, monoclonal; WB, Western blot; ICC, immunocytochemistry; IP, immunoprecipitation.

by sequencing. For immunocytochemistry, COS-7 cells were seeded onto poly-L-lysine-coated (Sigma Aldrich, St. Louis, MO, USA) cover slips and transfected with calcium phosphate transfection as described previously.<sup>37</sup> Briefly, 2X BBS buffer containing 50 mM BES, 280 mM NaCl, 1.4 mM Na<sub>2</sub>HPO<sub>4</sub>, and pH 6.96 with 250 mM CaCl<sub>2</sub> was incubated with vector (2 µg/well) for 30 minutes and then added to the media (Dulbecco's modified Eagle's medium [DMEM] +10% fetal bovine serum [FBS]) on 70% confluent cultures. The next day, the media containing the transfection reagents was replaced and allowed to sit overnight prior to harvesting and downstream processing. For immunoprecipitation and Western blot, HEK 293T cells were co-transfected using the same method. Cells were harvested (for Western blot) or fixed (for immunocytochemistry) 48 hours after transfection.

### Protein Analysis

For protein analysis, transfected HEK 293T cells were washed with 1x PBS, scraped into solubilization buffer (PBS, pH 7.0, containing 1% [v/v] TX-100, 5 mM EDTA, 5 mg/mL N-ethyl maleimide [NEM], and protease inhibitors), briefly sonicated and then incubated at 4°C for 1 hour. After pelleting insoluble material in a microfuge, soluble protein content in extracts was quantified using Bradford reagent (Bio-Rad) per the manufacturer's directions. Immunoprecipitation was performed using antibodies against Prph2 (100 µg protein extract per sample) and reducing SDS-PAGE/Western blot were performed as described previously.<sup>12,19,38</sup> Table 1 lists the primary antibodies used; the secondary antibodies were anti-mouse 800IR/anti-rabbit 680IR (Licor, Lincoln, NE, USA). Contrast and brightness were increased (uniformly across the whole blot) to improve visualization.

### Immunocytochemistry

Transfected COS-7 cells were washed with 1x PBS and then fixed in 4% paraformaldehyde for 20 minutes at room temperature. For immunolabeling, cells were washed in PBS then blocked for 1 hour in blocking buffer (10% donkey serum, 1% fish gelatin, 5% bovine serum albumin, and 0.2% Triton X-100 in PBS). Cells were incubated in primary antibodies (see Table 1) in blocking buffer overnight at 4°C. Cells were then washed in PBS, incubated with appropriate AlexaFluor-conjugated secondary antibodies (Thermo Fisher), rinsed again, and mounted using ProlongGold mounting medium containing 4',6-diamidino-2-phenylindole (DAPI; Thermo Fisher). Images were captured on a BX-62 spinning disk confocal microscope equipped with an ORCA-ER camera (Olympus, Japan) and analyzed with Slidebook 5 software (Intelligent Imaging Innovations, Denver, CO, USA). Images were captured with a 100x/1.40 oil objective, and exposure times and display settings (brightness and contrast) for all images were normalized to a control

section where primary antibody was omitted during processing. No gamma adjustments were made to immunofluorescent images.

## RESULTS

### Retinal Function is Impaired in Patients With the P210R Mutation

To understand the pathophysiological effect of the missense mutation c.629C>G, p.Pro210Arg (or P210R) in *PRPH2*, we evaluated 11 patients from 7 families who were previously determined to harbor this mutation. The age of onset was not recorded for most of the patients but the clinical notes indicated that the subjective onset of visual abnormalities was highly variable, ranging from childhood (e.g. C1) to adulthood (e.g. A2; Table 2). Additionally, Table 2 lists the age of each patient at the most recent visit, clinical diagnosis, BCVA (Snellen), refraction, and the results from color vision testing (Farnsworth D-15). The subjects' age at the most current visit ranged from 33 to 72 years (mean 49 ± SD 14 years). Patients were diagnosed with either adPD or macular dystrophy (adMD). Two patients (C1 and D1) were initially diagnosed with Stargardt disease (STGD1). Because STGD1 is exclusively associated with the gene *ABCA4*, the diagnosis for these two patients changed to adMD after genetic testing, which revealed the presence of the P210R mutation in *PRPH2* without additional mutations detected in *ABCA4*. Through segregation analysis of the P210R mutation among family members, subject # A3, the daughter of patient A1 and subject # A4, the son of patient A2, were found to carry the family mutation but neither were aware of visual abnormalities at the time of genetic testing. In this cohort, the patients' BCVA ranged from 20/15 in one patient (A4) to 20/80 in the oldest patient (E1). All subjects except A3, A4, D2, and G1 performed the Farnsworth D-15 color discrepancy test. The results for patient A1 showed Tritanomaly, A2 trended toward Tritan, and E1 was Protanomaly. The remaining four subjects (B1, C1, D1, and F1) had normal color discrimination (see Table 2).

Because *PRPH2* mutations are well-known to cause both rod-dominant and cone-dominant diseases, we next analyzed the clinical results from electroretinography (ffERG and mfERG). Some data were acquired at a visit prior to the most recent visit. In these cases, the age of the patient at that visit is provided in parentheses (Table 3). Of those tested with ffERG ( $n = 8$ ), there were four subjects (B1, D2, F1, and G1) with normal rod and cone responses and four (A1, A2, C1, and D1) with cone responses that were affected to a greater extent than the rod responses (see Table 3). Figure 1A shows representative ffERG responses from the left eye (OS) of patient C1, which revealed the rod response (top waveform) was within normal limits (WNLs) and the cone response (bottom waveform, black line) was

**TABLE 2.** Age of Each Patient at the Most Recent Visit, Clinical Diagnosis, BCVA (Snellen), Refraction, and the Results From Color Vision Testing

Patient	Age: Visit/Onset	Gender	Diagnosis	BCVA OD; OS	Refraction	Color Test
A1	65 y/Childhood	F	adPD	20/25 OU <sup>33</sup>	+0.50 + 0.75 × 174; -0.75 + 1.00 × 170 <sup>33</sup>	Tritanomaly or Tritanopy OD
A2	60/50 y	M	adMD	20/40; 20/50 <sup>34</sup>	Plano	Probably normal OD; trended toward Tritan ND
A3	34 y/NA	F	At risk	20/20 OU	Plano	ND
A4	33 y/NA	M	At risk	20/15 OU	Plano	ND
B1	43 y/UK	M	adMD	20/25; 20/32	Unknown	Normal OS
C1	33 y/Childhood	F	STGD1/ adMD	20/20; 20/63	-4.50 + 1.50 × 100; -3.75 + 1.75 × 076	Normal OD
D1	57 y/UK	F	STGD1/ adMD	20/40; 20/80	Contacts	Normal OS
D2	30 y/30	F	adMD	20/32 OU	Plano	ND
E1	72 y/UK	F	adPD	20/32; 20/80	-2.75 + 0.75 × 152; -4.25 + 1.25 × 017	Protanomaly OS
F1	59 y/UK	F	adMD	20/63 OU	0.25 + 0.50 × 131; 0.25 + 0.50 × 039	Normal OD
G1	50 y/49	F	adMD	20/32; 20/25	Unknown	ND

BCVA, best corrected visual acuity; NA, not applicable; UK, unknown; ND, not done; OU, both eyes; OD, right eye; OS, left eye; ad, autosomal dominant; PD, pattern dystrophy; MD, macular dystrophy; STGD1, Stargardt disease.

**TABLE 3.** Results From Electroretinography (ffERG and mfERG)

Patient	ffERG	mfERG	DAC			Kinetic Visual Field (VF)	Humphrey 30-2 (MD, dB)	Octopus900
			Central (% Abnormal; MD)	DAC Mid (% Abnormal; MD)	DAC Far (% Abnormal; MD)			
A1	Normal but delayed rod response; decreased and delayed cone response OS	OU reduced (age 58 y)	99%; -14 dB OS	Normal OS	Normal OS	Para-central IN scotoma OD	-3.70 OD (age 58 y)	ND
A2	Normal but delayed rod response; decreased and delayed cone response OS	ND	Normal OS	8%; -2 dB OS	Normal OS	Full OD	-1.82 OD (age 56 y)	reduced/scotomas SN, ST, and IT OS
A4	ND	ND	Normal OS	Normal OS	25%; -5.3 dB OS	Full OD	ND	Reduced/scotomas SN, ST, and IT OS
B1	Normal OD	ND	58%; -2 dB OD	11%; -7 dB OD	25%; -17 dB OD	Full OS	-0.25 OS (age 41 y)	ND
C1	normal rod response; decreased and delayed cone response OS	OU reduced (age 27 y)	100%; -27 dB OS	94%; -7 dB OS	50%; -12 dB OS	Crescent scotoma in macula OD	-14.24 OD (age 27 y)	Scotomas S and T and crescent scotoma in macula OS (age 31y)
D1	Normal rod response; normal but delayed cone response OD	OD normal; OS reduced (age 48 y)	Normal OD	10%; -27.3 dB OD	25%; -19 dB OD	Full OS	-3.61 OS (age 48 y)	Reduced/scotomas SN, ST, and IT OD
D2	Normal OS	ND	ND	ND	ND	Full OD	ND	ND
E1	ND	ND	94%; -10 dB OD	56%; -13 dB OD	92%; -12 dB OD	ND	ND	ND
F1	Normal OS	ND	Normal OS	Normal OS	Normal OS	Full OD	ND	Reduced/scotomas SN, ST, and IT OD
G1	Normal OD	OD reduced; OS ND	ND	ND	ND	ND	ND	ND

Note: These examinations were unavailable for patient A3.

ND, not done; MD, mean deviation of abnormal loci from the lower limits of age/location-corrected normal values; mid, mid-peripheral; far, far-peripheral; I, inferior; N, nasal; T, temporal; S, superior; OU, both eyes; OD, right eye; OS, left eye.

subnormal (dashed line) in amplitude. Seven eyes from four subjects (A1, C1, D1, and G1) received an mfERG to test the cone responses at the central 30 degrees of the macula. The mfERG results revealed reductions in response densities (see Fig. 1B, right eye [OD] for patient G1) compared to normal reference responses (see Fig. 1C) in five (out of 7) eyes (see Table 3). All of the reductions were found in the foveal responses and in areas that correspond to atrophy (hypo-AF) on retinal images. Recordings from ERG suggest that the P210R mutation in PRPH2 is primarily detrimental to the cone photoreceptors compared to the rod photoreceptors. To further delineate the effect of the P210R mutation in PRPH2 on rod and cone function, perimetry examinations were performed to determine visual field (VF) defects under dark-adapted and room lighting conditions. Of those who completed dark-adapted static perimetry (DAC testing) of the full retina ( $n = 8$ ; see Table 3), only patient F1 had

normal sensitivity at all test points throughout the VF (not shown). Figure 2 shows the heat maps of rod sensitivities (dB) for patients A1 (A), A2 (B), A4 (C), C1 (D), B1 (E), D1 (F), E1 (G), and a normal control (H). Additionally, we compared the mean local sensitivity (dB) to stimuli testing points in the central retina, mid-peripheral, or far-peripheral retina to age-matched normal control sensitivities.<sup>34</sup> Of the eight patients who received DAC testing, four (A2, A4, D1, and F1) had normal sensitivity for all loci tested in the central retina whereas the remaining four (A1, B1, C1, and E1) had sensitivity below normal (average mean deviation [MD] -13 dB ± 9 STDV) for the majority (58–100%) of the loci tested. For the mid- and far-peripheral loci, the average MD was -11 ± 9 dB ( $n = 5$ ) and -13 ± 5 dB ( $n = 5$ ) below normal, respectively, which represented defects from 8% to 94% and 25% to 92% of the tested loci, respectively (see Table 3). These data indicate that the P210R PRPH2 mutation also

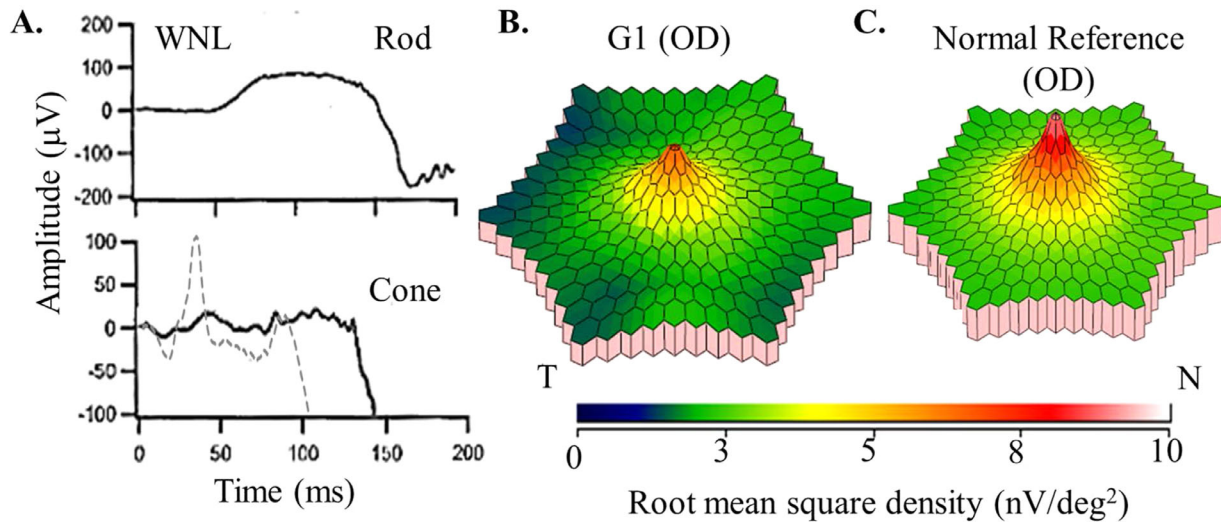


**FIGURE 1. Representative electroretinography responses.** (A) The fERG responses from the left eye (OS) of patient C1 rod response (*top*) amplitude within normal limits (WNL) and decreased amplitude for the cone response (*bottom; solid black line*) compared to normal (*gray dashed line*). (B) The mERG of the right eye (OD) from patient G1 revealed reduced amplitudes compared to the (C) normal reference response densities. N, nasal; T, temporal.

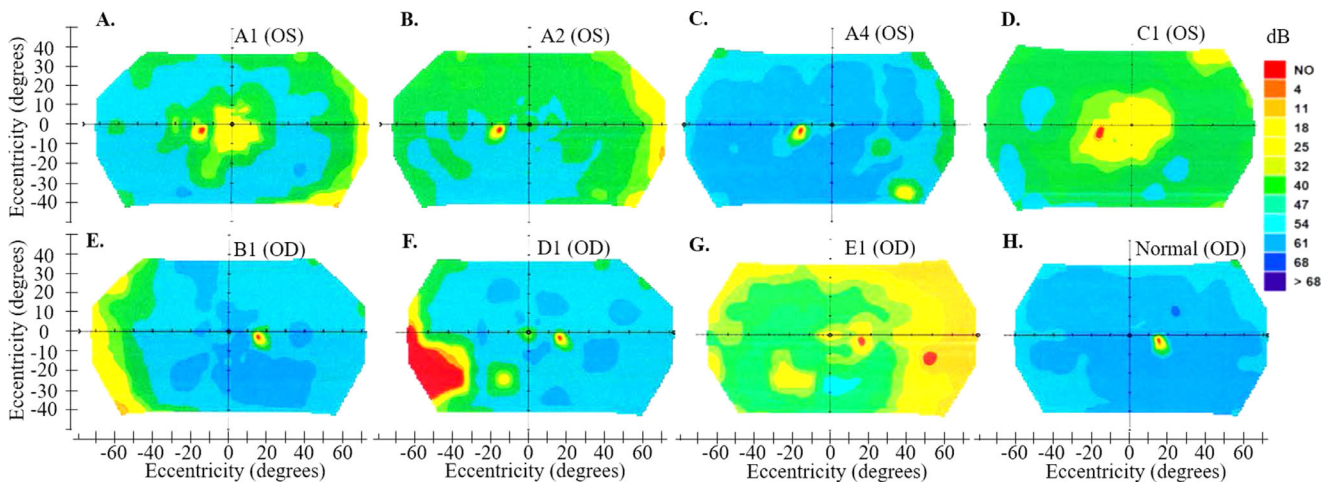


**FIGURE 2. Dark-adapted chromatic perimetry results showing rod sensitivity measured throughout the visual field.** Sensitivity (dB) of loci tested in the left eyes (OS) of patients A1 (A), A2 (B), A4 (C), and C1 (D). Sensitivity of loci tested in the right eyes (OD) of patients B1 (E), D1 (F), and E1 (G), and a 43-year-old normal-sighted control. *Blue colors* indicate better rod function whereas *red areas* specify loci that were not detected with the brightest intensity of the stimulus. Eccentricity 0, 0 was the position of the fovea. The blind spot in the field is the red spot slightly below the horizontal midline at  $-10$  degrees to  $-15$  degrees OS or  $10$  degrees to  $15$  degrees OD. No (*red*), or 0 dB means that the patient did not see the stimulus at the brightest intensity.

causes localized functional abnormalities in rod photoreceptors not detectable by fERG.

Kinetic and static perimetry were examined to determine if VF defects were related to cone-mediated vision. Overall, the kinetic VFs were full (similar to a normal VF) or slightly reduced compared to normal (see Table 3) in patients carrying the P210R PRPH2 mutation. Additionally, two subjects (A1 and C1) had scotomas in the central field that were mapped with multiple perimetric examinations (see Table 3). Although kinetic VFs were full, static perimetry revealed a universal and generalized reduction in sensitivity in the central (HFA and Octopus 900) and the far peripheral VFs (Octopus 900). Altogether, the perimetry outcomes showed retina-wide dysfunction of rods and cones with increased damage localized to the macula and far peripheral VF.

### P210R Retinas Exhibit Structural Abnormalities Characteristic of Retinal Degeneration

After we evaluated the visual and photoreceptor function from patients with the P210R mutation in PRPH2, we assessed retinal structure using fundus photography (pseudo color and autofluorescence [AF]) and SD-OCT imaging. Fundus images were available for A1, A2, C1 (left eyes shown in Fig. 3A), and E1 (not shown), which demonstrated a spectrum of clinical features associated with this mutation. The fundus appearance of patient A1 showed confluent areas of chorioretinal atrophy concentrated within the posterior pole, whereas her brother (A2) had a relatively normal fundus image (see Fig. 3A). Patient C1 had fundus abnormalities, including multifocal areas of chorioretinal

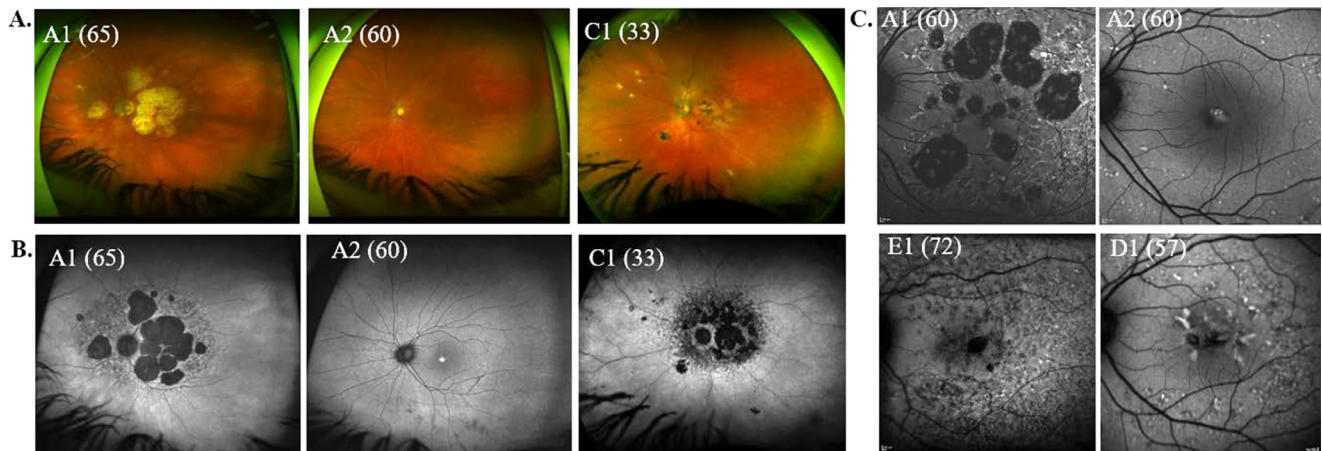


**FIGURE 3.** Left eye fundus images from patients with the P210R mutation in *PRPH2*. (A) Wide-field pseudo-colored and (B) autofluorescent (AF) images from patients A1, A2, and C1. (C) Blue-wavelength AF images from patients A1 (age 60 years), A2, E1, and D1. Patient age when the image was acquired is in parentheses.

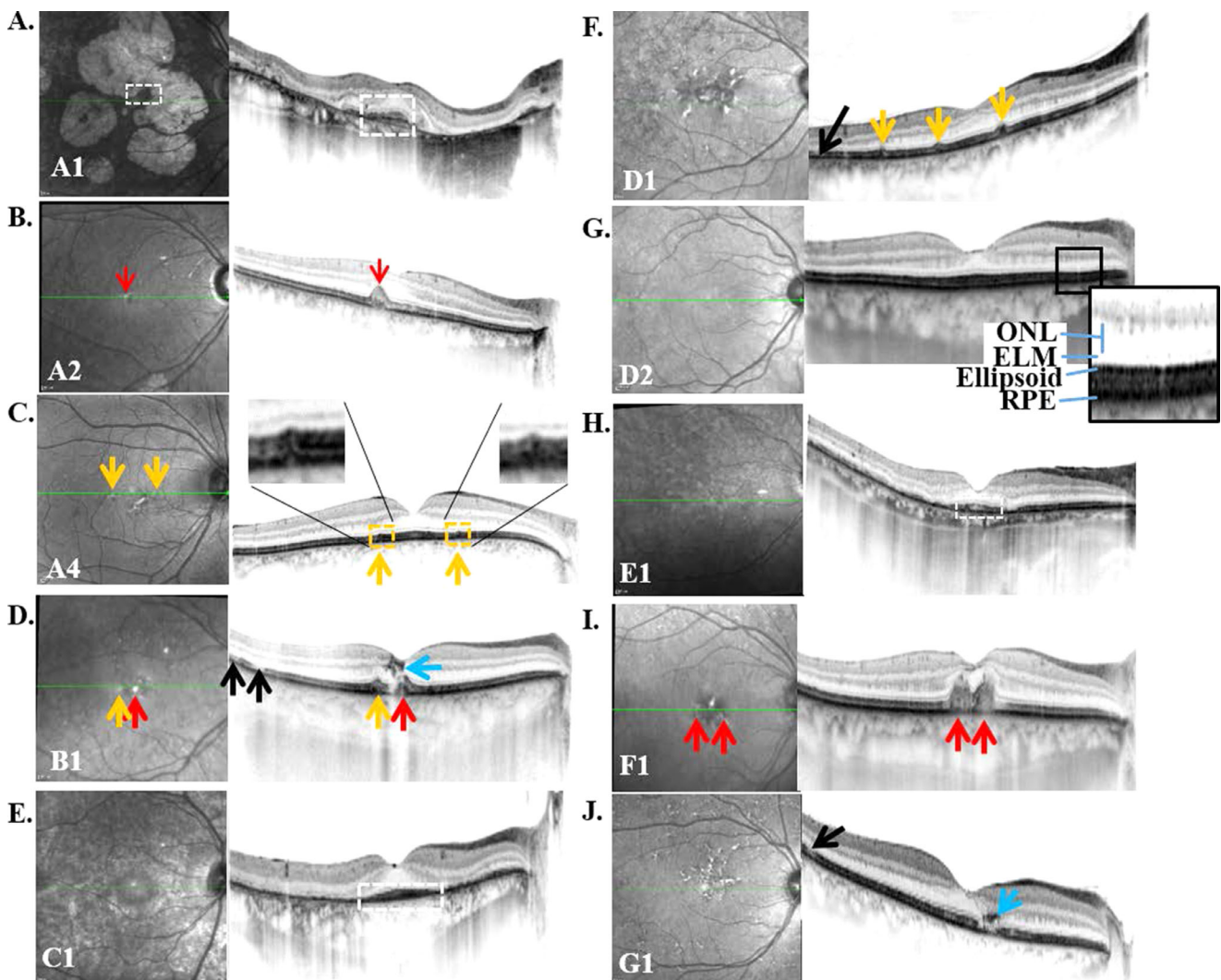


**FIGURE 4.** Right eye spectral-domain optical coherence tomography (SD-OCT) images from patients with the P210R mutation in *PRPH2*. NIR images (left) showing the horizontal axis (green line) of the scan position of the SD-OCT images (right) from patients A1 (A), A2 (B), A4 (C), B1 (D), C1 (E), D1 (F), D2 (G), E1 (H), F1 (I), and G1 (J). Note that SD-OCT was not obtained for patient A3. White boxes, foveal sparing; red arrows, foveal drusen; yellow arrows, parafoveal drusen; black arrows, breaks in the photoreceptor inner/outer segment (ellipsoid) junction; blue arrows, migrating retinal pigment epithelium (RPE). Outer nuclear layer (ONL), and external limiting membrane (ELM).

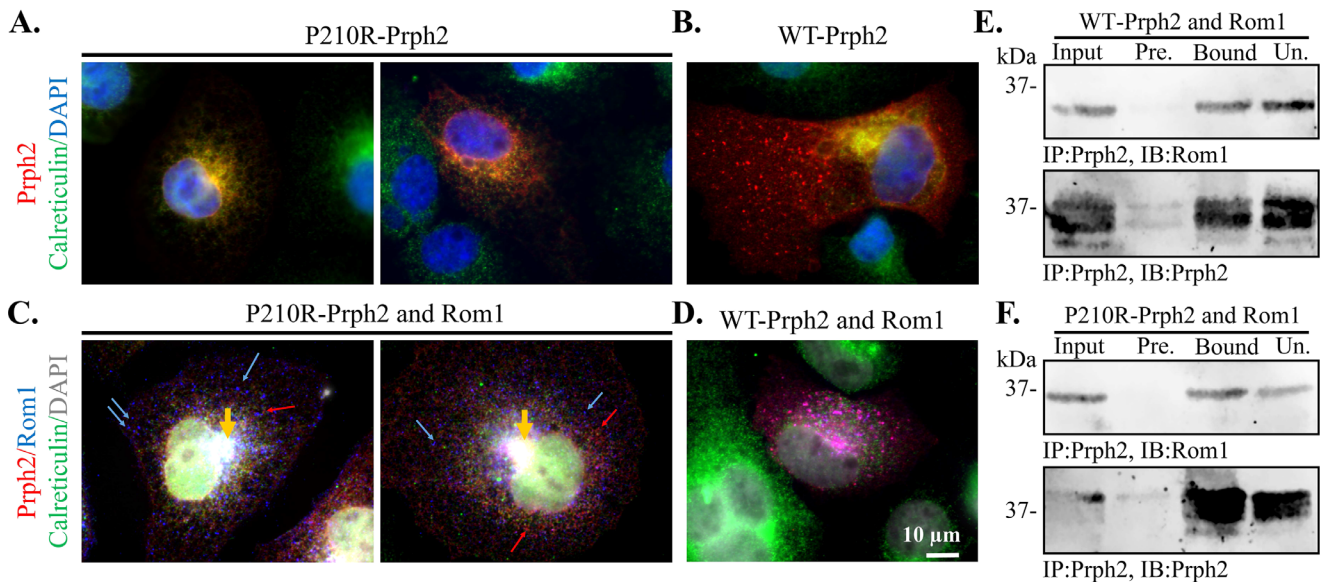


**FIGURE 5. P210R Prph2 retains the ability to bind Rom1 but accumulates abnormally in the ER.** COS-7 cells were single transfected with P210R-Prph2 (A) or WT-Prph2 (B), and cells were labeled for Prph2 (red) and the ER marker calreticulin (green); and nuclei are counterstained with DAPI (blue). P210R accumulated in the ER (yellow), in contrast to WT-Prph2 (red) which was distributed in punctae throughout the cell. (C-D) COS-7 cells were double transfected with P210R-Prph2 (C) or WT-Prph2 (D) and Rom1 and labeled for Prph2 (red), Rom1 (blue), and calreticulin (green); and the nuclei are counterstained with DAPI (grey). WT-Prph2 and Rom1 co-localized (magenta) with very little found in the ER (green). P210R-Prph2 and Rom1 exhibited some co-localization in the ER (white signal, orange arrow), and the small amount of P210R that exited the ER (red, red arrows highlight examples) did not appear to co-localize with Rom1 (blue, blue arrows highlight examples). Images captured at 100x, scale bar is 10  $\mu$ m for all images, A and C show two different representative cells. (E-F) HEK 293T cells were co-transfected with P210R-Prph2 and Rom1 (E) or WT-Prph2 and Rom1 (F). Prph2 antibodies (RDS-CT) were used to immunoprecipitated (IP) Prph2 complexes from cell lysates. Blots were immunoblotted (IB) for Prph2 or Rom1. Input, starting lysate; Pre., preclear; beads + IgG; Bound, fraction bound to Prph2 antibody; Un., unbound flow through.

atrophy and pigment clumps extending to the mid-periphery (see Fig. 3A). Optos AF images showed significant hypo-AF regions of retina and retinal pigment epithelium (RPE) atrophy in the posterior pole with peripapillary sparing for patients A1 and C1, whereas patient A2 only showed focal foveal hyper-AF (see Fig. 3B). Also presented in Figure 3 are the blue-wavelength AF images from the left eyes (OS) showing hyper-AF flecks in the macula but the patterns of AF were dissimilar (see Fig. 3C). The blue-wavelength AF image for patient A1 at age 60 years (see Fig. 3C) demonstrated multiple atrophic lesions that expanded and coalesced by age 65 (see Figs. 3A, 3B). In contrast, patient E1 demonstrated diffuse punctate areas of hypo-AF interspersed with hyper-AF flecks, and patient D1 displayed a Stargardt-like hyper-AF pattern in the macula (see Fig. 3C). In summary, the fundus evaluations provided evidence for the heterogeneous structural damage to the RPE and retina when an individual harbors the P210R mutation in *PRPH2*.

To assess the retinal layers in greater detail, macula scans from SD-OCT were available for examination for all subjects except A3 (Fig. 4). A near-infrared reflectance (NIR) image (left panel) acquired simultaneously shows the location of the horizontal line scan through the fovea (green line) of the SD-OCT image (right panel). Patient A1 had atrophy of the outer retinal layer with a relatively spared foveal island (see white box in Fig. 4A). For patient A2, the central hyper-AF signal was revealed as subfoveal drusen (red arrow), with distortion of the normal foveal contour (see Fig. 4B). The son of A2, patient A4, had small reflective pisciform deposits on the NIR image (left panel, yellow arrows) corresponding to small juxtafoveal RPE deposits with elevated/intact overlying

ellipsoid (yellow arrows; insets) on SD-OCT (see right panel in Fig. 4C). Patient B1 had subfoveal (red arrows) and juxtafoveal (yellow arrows) deposits associated with breaks in the ellipsoid band and pigment migration (blue arrow), as well as temporal ellipsoid band disruptions not obviously associated with subretinal deposits (see black arrows in Fig. 4D). Patient C1 (see Fig. 4E) had foveal sparing of the ellipsoid band (white box), with irregularities of nasal ellipsoid band and degeneration of the temporal outer retina (see Fig. 4E). Patient D1 had small juxtafoveal drusen (yellow arrows) along with a break in the temporal aspect of the ellipsoid band (see black arrow in Fig. 4F). However, her daughter, patient D2, did not have any obvious retinal changes on SD-OCT and this image was therefore used to illustrate the magnified retinal layers (see inset in Fig. 4G). Patient E1 had temporal outer retinal thinning with foveal sparing (see white box in Fig. 4H). Confluent subfoveal drusen (red arrows) were found on the SD-OCT image from patient F1 (see Fig. 4I). Finally, ellipsoid band disruption was detected temporally and juxtafoveally (black arrows) with pigment migration (blue arrow) in patient G1 (see Fig. 4J). Altogether, the right eye SD-OCT line scans through fixation revealed heterogeneous outer retinal changes with or without foveal sparing (see Fig. 4).

#### P210R-Prph2 Retains the Ability to Interact With Rom1, but Accumulates in the ER

To help understand the molecular and cellular effects of the P210R mutation we undertook in vitro evaluation of P210R

Prph2 mutant protein. To evaluate whether P210R Prph2 could traffic out of the ER, COS-7 cells were single transfected with *P210R-Prph2* (Fig. 5A) or *WT-Prph2* (Fig. 5B). Cells labeled for Prph2 (red) and the ER marker calreticulin (green) showed that P210R-Prph2 largely accumulated in the ER (see yellow in Fig. 5A). In contrast, WT-Prph2 was largely distributed as expected outside the ER, in punctae throughout the cell (see red in Fig. 5B). Previous studies testing different mutations showed that accumulation of some mutant Prph2 proteins in the ER was decreased by the presence of Rom1,<sup>19</sup> so we asked whether the localization of P210R-Prph2 was altered by co-expression with Rom1. COS-7 cells were double transfected with *Rom1* and *P210R-Prph2* (Fig. 5C) or *WT-Prph2* (Fig. 5D). Cells were labeled for Prph2 (red), Rom1 (blue), and calreticulin (green). P210R-Prph2 and Rom1 exhibited co-localization in the ER (orange arrows highlight white signal resulting from red/green/blue overlap in Fig. 5C) whereas WT-Prph2 and Rom1 were co-localized (magenta) throughout the cytoplasm with very little detected in the ER (see green in Fig. 5D). These results suggest that the P210R-Prph2 contributed to abnormal accumulation of Rom1 in the ER. In addition, there was some P210R-Prph2 and Rom1 detected outside the ER, but they did not co-localize (note distinct red and blue punctae, some examples highlighted with arrows of respective colors in Fig. 5C). These data suggest that P210R promotes abnormal folding and ER retention of Prph2 and may also lead to the sequestration of Rom1 in the ER. To determine whether the P210R mutation affected the ability of Prph2 and Rom1 to oligomerize, we performed immunoprecipitations (IPs) followed by Western blot analysis on lysates from HEK293T cells that had been co-transfected with *Rom1* and either *P210R-Prph2* (Fig. 5E) or *WT-Prph2* (Fig. 5F). Using an antibody against the Prph2 C-terminal, IP pulled down Rom1 and both P210R-Prph2 (see Fig. 5E) and WT Prph2 (see Fig. 5F), suggesting that the P210R mutation does not block the ability of Prph2 and Rom1 to oligomerize.

## DISCUSSION

Here, we have demonstrated the clinical features associated with eleven patients who harbor the P210R mutation in *PRPH2*. Recently, Oishi et al.<sup>39</sup> reported that the missense mutation P210R causes autosomal dominant RP.<sup>15</sup> This clinical diagnosis was likely based on the observation of pigment clumping that occasionally occurs in these patients (see Fig. 3A, patient C1). However, the patients in the present cohort had features of macular dystrophy (adMD or adPD) whereas patients with RP classically show bone spicules, arteriole narrowing, and optic nerve pallor. Based on our present findings, we conclude that the P210R mutation in *PRPH2* is associated with a clinical diagnosis of dominantly inherited maculopathy (adMD or adPD).

Patients with cone-associated mutations in *PRPH2* are often clinically diagnosed with STGD1 before the genetic diagnosis is confirmed. This is likely due to the phenotypic similarities on funduscopy and lack of clinical tests that can accurately differentiate these diseases. A difference between STGD1 and *PRPH2*-associated maculopathy is that STGD1 is classically an early onset (childhood) autosomal recessive IRD due to bi-allelic mutations in the gene *ABCA4* whereas *PRPH2*-related retinopathy is autosomal dominant (or digenic) and the disease onset can begin as early as childhood but is more often delayed until adulthood. However, it should be noted that adult onset STGD1 is not uncom-

mon and *PRPH2*-related IRD can present as simplex due to reduced penetrance and/or subclinical disease which adds to the difficulty in differentiating the diseases prior to genetic testing. Within our cohort, the age of onset was unknown for the majority of patients (see Table 2). Because of the dominant inheritance of *PRPH2*-associated disease, families with a known mutation are more likely to be vigilant at monitoring their child's vision and therefore a diagnosis would be sought at an earlier age. However, for those without a known family history, diagnosis may be delayed due to the slow onset and insidious progression of disease, thus complicating correlation of age-of-onset with patient genotype. Visual function appears largely preserved in patients harboring the P210R mutation in *PRPH2*, except in cases with foveal involvement (e.g. A2 or F1; see Figs. 4B, 4I). Patients A3 and A4 denied vision problems, and only mild defects were observed for patient A4, such as slight reductions in rod and cone sensitivities (see Table 2; Fig. 2C), as well as early evidence of drusen on SD-OCT imaging (see Fig. 4C). Often, patients with *PRPH2*-related disease have fERG responses within the normal range.<sup>36</sup> However, as the disease evolves, ERG defects can begin to appear, and the ERG data presented for the current group of patients suggest that photoreceptor dysfunction occurs in cones prior to rods for patients harboring the P210R mutation in *PRPH2*.

Tritan defects (loss of short wavelength cones) are known to be associated with acquired color blindness in patients with RP<sup>40</sup> and as a result of aging ( $\geq 70$  years).<sup>41</sup> Additionally, cataracts, glaucoma, and age-related macular degeneration can also cause someone to test with Tritanomaly. Siblings A1 and A2 had a family history of glaucoma and were the only subjects with Tritan abnormalities. The oldest patient in this cohort (72 years) was E1 who tested with Protanomaly. Protanopia is a complete loss of the normal function of long wavelength cones (L-cones), meaning that the patient did not see red hues. Protanomaly has been associated with progressive cone dystrophies and RPE dystrophies.<sup>42</sup> Although one patient does not provide unequivocal evidence, the color discrimination test results could mean that the P210R mutation may be detrimental to the red cones at later stages of the disease in the absence of additional eye disease (such as glaucoma)<sup>43–46</sup> contributing to blue cone pathology. More research is needed to test this theory. Interestingly, in *Rds* heterozygous mice (*Rds*/+, a loss-of-function RP model), the red/green cones were more vulnerable to deterioration than the blue cones.<sup>47</sup> However, this does not occur in all cases, and in several *Prph2* mouse models carrying mutations that lead to severe defects in cone function (e.g. R172W, K153del, and C213Y) both short-wavelength (UV) and long wavelength (red/green) cones are similarly affected.<sup>26,29,48</sup> However, care must be taken when applying these findings to human patients, as most mouse cones express both S- and M- opsins (rather than a single cone opsin type).<sup>49,50</sup> In addition, the evaluation of S- versus M- cone function in murine *Prph2* models was done at earlier ages (1–6 months) so it is possible that preferential effects on one cone subtype could occur at later ages.

ABCA4 is an ATP-binding cassette (ABC) superfamily transmembrane protein that is responsible for clearance of all-*trans*-retinal aldehyde-phosphatidylethanolamine (retinaldehyde-PE), a byproduct of the phototransduction process.<sup>51</sup> In the presence of bi-allelic mutations in *ABCA4*, the retinaldehyde-PE accumulates in the form toxic vitamin A dimers such as *N*-retinylidene-*N*-retinylethanolamine (A2E) that comprise lipofuscin which are then deposited

in the RPE after phagocytosis of the photoreceptor outer segments. Fundus hyper-AF flecks are associated with both STGD1 and *PRPH2*-associated disease. In STGD1, the hyper-AF flecks arise from the reflective lipofuscin granules that accumulate in the RPE. The reason for the formation of drusenoid deposits in patients with a *PRPH2* mutation has yet to be determined. Because both *PRPH2* and *ABCA4* are localized to the outer segment rim, one possibility is that the mutant *PRPH2* sequesters *ABCA4* in the ER, therefore reducing the clearance of toxic byproducts of phototransduction and the accumulation of lipofuscin that are found in drusen. An alternative hypothesis is tied to the abnormal structure of outer segment discs in *Prpb2* mutant models. Animal models have shown that most *PRPH2* mutations lead to the formation of abnormal whorl shaped outer segments in which discs are highly elongated (prompting the swirl pattern), rather than stacking nicely in a columnar outer segment. Such an arrangement would increase the distance between *ABCA4* protein (at the disc rim) and the phototransduction components that are distributed throughout the disc. Both options would help explain the later onset of *PRPH2*-related IRD compared to STGD1, because in both cases some level of *ABCA4* would still be available in the outer segments, even if at reduced levels. The fovea is comprised of cone receptors for high visual acuity so that the region of the retina has very high energy demand and high levels of visual pigment turnover. As a result, the deleterious effects of drusen are exacerbated in the fovea and play a key role in diseases such as STGD1. However, in contrast to the usual case in STGD1, most patients in our P210R *PRPH2* cohort had some level of foveal sparing except for patients A2 (OU), B1 (OU), E1 (OS), and F1 (OS; see Fig. 4 and Supplementary material), highlighting additional differences between *PRPH2*-associated disease and *ABCA4*-associated disease. The patients without foveal sparing in the right eyes (A2 and B1) were affected with foveal drusen. The left eyes of E1 and F1 had foveal atrophy, which may indicate localization of resolved drusen. An alternative mechanism for *PRPH2* disease phenotypes in the RPE could be tied to the build-up of abnormal mutant *PRPH2* complexes and associated abnormal outer segment structures, and thus be independent of *ABCA4*. The RPE phagocytoses and degrades large quantities of lipid and protein as part of outer segment turnover, and it is not clear to what extent the ability of the RPE to perform this role effectively may be altered by the accumulation of mutant *PRPH2* protein complexes and/or abnormal outer segment structures. However, this would not explain the hyper-AF drusen associated with the P210R mutation.

Mouse models have revealed that *PRPH2* plays a different role in rod vs. cone photoreceptors. In *Prpb2* knock out mice, rod outer segments fail to form<sup>1</sup> whereas cone outer segments retain balloon-like membranous lamellae that lack rims but retain the ability to mediate phototransduction.<sup>52</sup> Yet, it is still unclear why some *PRPH2* mutations result in rod dominant retinal disease (adRP) whereas others, such as P210R, lead to a cone phenotype (adMD or adPD). Data from animal models have suggested that loss-of-function mutations and resulting haploinsufficiency initially target rods with cone defects developing later, whereas dominant-negative or gain-of-function mutations often lead to initial cone-dominant defects with rod changes occurring subsequently. For rod receptors, it has been previously determined that normal outer segment structure requires 60% to 80% of normal *PRPH2* protein,<sup>47,53,54</sup> and that reduced

*PRPH2* levels lead to earlier onset defects in rod structure and function. In contrast, data from mouse models suggest that *PRPH2* mutations that lead to abnormalities in *PRPH2*-ROM1 complex assembly are more deleterious to cones than rods.<sup>47,55,56</sup> Interestingly, human patients with a heterozygous deletion of *PRPH2* results in macular disease. Although the specific mechanisms underlying these species differences are unknown, one critical difference between the mouse and human retina is the lack of a macula in mice, making it difficult to specifically model macular disease mechanisms. Further evaluation is clearly needed to fully comprehend how different mutations, modifiers, or protein levels affect rod and cone photoreceptors both inside and outside the macula.

Previous studies using mouse models and cultured cells have shown that *Prpb2* mutations can lead to diverse molecular and cellular effects, including impaired protein folding, impaired protein trafficking, and impaired *Prpb2*-Rom1 complex assembly, all of which can contribute to structural and functional defects in rod and cone photoreceptors.<sup>14,19,31</sup> Initial *PRPH2* complex assembly with ROM1 begins in the inner segment where the two proteins form homo- and hetero-tetramers which then traffic to the outer segments. Once in the outer segment, they assemble into higher complexes held together by intermolecular disulfide bonds.<sup>6,12,57</sup> *PRPH2*-ROM1 noncovalent interactions occur in the first half of the *PRPH2* D2 loop (Tyr140-Asn182),<sup>10</sup> so it is not surprising that our in vitro data show that P210R-*PRPH2* retains the ability to interact with ROM1. However, accumulation of the mutant P210R protein (and retention of some ROM1) in the ER suggest that the P210R mutation may contribute to misfolding of other parts of the D2 loop and subsequent abnormalities in the assembly of larger *PRPH2*-ROM1 complexes. This hypothesis is consistent with our observations from other *PRPH2* mutants,<sup>19</sup> but further evaluation of the molecular and biochemical effects of the P210R mutation would require a more tissue-like environment, such as a mouse model or patient-derived retinal organoid. Many *PRPH2* mutants cause rod and cone disease in both humans and animal models.<sup>15,29,31</sup> We found that in several of the P210R patients as well, for example, patients with adMD or adPD due to the P210R mutation in *PRPH2* also exhibited rod dysfunction (see Table 3, Fig. 2). Together, these results suggest that the P210R mutation may lead to diminished ability to form stable, correctly assembled *PRPH2*-ROM1 complexes thus leading to defects in both rods and cones.

The role of ROM1 and other potential modifier genes is also worth exploring. Single ROM1 mutations are not pathogenic, but the *PRPH2* mutation, c.554T>C (p.Leu185Pro), causes adRP only in digenic situations when the patient also harbors one of three known variants in the *ROM1* gene.<sup>17</sup> The three known *ROM1* variants digenic with *PRPH2* are two frameshift mutations and a p.Gly113Glu mutation.<sup>16,17</sup> This digenic inheritance is relatively rare, accounting for 0.5% to 3% of cases of patients with dominant or recessive RP in a population of predominantly European origin.<sup>16</sup> Because many *PRPH2* disease mutations are associated with a high degree of inter-family phenotypic heterogeneity, there has also been interest in exploring the role of potential modifier genes. Potential modifier genes/alleles explored thus far include single nucleotide polymorphisms in *ROM1*, *PRPH2* haplotypes in trans, and variants in *ABCA4*.<sup>19,20,58</sup> The increased availability of next generation sequencing has increased the ease with which

novel variants can be identified, and more and more complex IRD inheritance patterns continue to emerge in which multiple pathogenic mutations are present.<sup>4,19,20</sup> In this work, we did not investigate the potential disease modifying effect of *ROM1* variants. Although none of the patients had “likely pathogenic” or “pathogenic” mutations in *ROM1*, common single nucleotide polymorphisms in *ROM1* (or aforementioned genes/alleles) that may modify the phenotype are not well-characterized and the number of patients here was too small for statistical evaluation of modifying effects.

In conclusion, we here present data showing that the P210R-*PRPH2* mutation is associated with decreased rod and cone sensitivity, but that vision loss was most pronounced in the macula, likely due to atrophy that occurs after drusen have formed and begin to resolve. Our in vitro data suggest that this may be tied to abnormalities in the folding and/or trafficking of P210R mutant *PRPH2*, and that experiments using more sophisticated model systems would be highly beneficial in further elucidating the cellular and molecular mechanisms of P210R-associated disease. However, the association of drusen with vision loss in these patients suggests that, in common with other *PRPH2* mutations, a full understanding of the disease process must include evaluation of secondary effects of photoreceptor abnormalities in the RPE.<sup>31,59,60</sup> Likewise, our findings suggest that although rod and cone photoreceptors are dependent on *PRPH2*, preventing blindness in this specific subgroup of patients could involve therapeutics to impede the lifecycle of drusen formation and subsequent atrophy.

### Acknowledgments

The authors thank Muna Naash (University of Houston, Houston, TX) for the provision of antibodies and constructs as indicated in the text.

Funded by the National Eye Institute at the National Institutes of Health (NIH), R00EY027460, R01AG070915, R01EY010609, and R01EY009076. This research was supported by the Oklahoma Center for Adult Stem Cell Research Grant Application (OCASCR) and the Oklahoma Shared Clinical and Translational Resources (U54GM104938) with an Institutional Development Award (IDeA) from NIGM. Oklahoma Center for the Advancement of Science and Technology (OCAST HR14-150). This work was supported in part by the NIH grant P30EY027125 (NIH CORE grant), by the Molecular and Cellular Imaging core and Animal Model Development and Behavioral Analysis cores that are part of 1P20GM125528 Cellular and Molecular GeroScience CoBRE, and an unrestricted grant to the Dean A. McGee Eye Institute from Research to Prevent Blindness Inc. (<http://www.rpbusa.org> accessed on 15 January 2019). The content is solely the responsibility of the authors and does not necessarily represent the official views of the National Institutes of Health.

Disclosure: **S.M. Conley**, None; **C.K. McClard**, None; **M.L. Mwoyosvi**, None; **N. Alkadhem**, None; **B. Radojevic**, None; **M. Klein**, None; **D. Birch**, None; **A. Ellis**, None; **S.W. Icks**, None; **T. Guddanti**, None; **L.D. Bennett**, None

### References

- Jansen HG, Sanyal S. Development and degeneration of retina in rds mutant mice: electron microscopy. *J Compar Neurol*. 1984;224:71–84.
- Molday RS, Hicks D, Molday L. Peripherin. A rim-specific membrane protein of rod outer segment discs. *Invest Ophthalmol Vis Sci*. 1987;28:50–61.
- Moritz OL, Molday RS. Molecular cloning, membrane topology, and localization of bovine rom-1 in rod and cone photoreceptor cells. *Invest Ophthalmol Vis Sci*. 1996;37:352–362.
- Jones KD, Wheaton DK, Bowne SJ, et al. Next-generation sequencing to solve complex inherited retinal dystrophy: A case series of multiple genes contributing to disease in extended families. *Mol Vis*. 2017;23:470–481.
- Chakraborty D, Conley SM, Fliesler SJ, Naash MI. The Function of Oligomerization-Incompetent RDS in Rods. *Adv Exp Med Biol*. 2010;664:39–46.
- Loewen CJ, Molday RS. Disulfide-mediated oligomerization of Peripherin/Rds and Rom-1 in photoreceptor disk membranes. Implications for photoreceptor outer segment morphogenesis and degeneration. *J Biol Chem*. 2000;275:5370–5378.
- Poetsch A, Molday LL, Molday RS. The cGMP-gated channel and related glutamic acid-rich proteins interact with peripherin-2 at the rim region of rod photoreceptor disc membranes. *J Biol Chem*. 2001;276:48009–48016.
- Tam BM, Moritz OL, Papermaster DS. The C terminus of peripherin/rds participates in rod outer segment targeting and alignment of disk incisures. *Mol Biol Cell*. 2004;15:2027–2037.
- Goldberg AF, Loewen CJ, Molday RS. Cysteine residues of photoreceptor peripherin/rds: role in subunit assembly and autosomal dominant retinitis pigmentosa. *Biochemistry*. 1998;37:680–685.
- Ding XQ, Stricker HM, Naash MI. Role of the second intradiscal loop of peripherin/rds in homo and hetero associations. *Biochemistry*. 2005;44:4897–4904.
- Goldberg AF, Molday RS. Subunit composition of the peripherin/rds-rom-1 disk rim complex from rod photoreceptors: hydrodynamic evidence for a tetrameric quaternary structure. *Biochemistry*. 1996;35:6144–6149.
- Chakraborty D, Ding XQ, Fliesler SJ, Naash MI. Outer segment oligomerization of Rds: evidence from mouse models and subcellular fractionation. *Biochemistry*. 2008;47:1144–1156.
- Chakraborty D, Ding XQ, Conley SM, Fliesler SJ, Naash MI. Differential requirements for retinal degeneration slow intermolecular disulfide-linked oligomerization in rods versus cones. *Hum Mol Genet*. 2009;18:797–808.
- Zulliger R, Conley SM, Mwoyosvi ML, Al-Ubaiddi MR, Naash MI. Oligomerization of Prph2 and Rom1 is essential for photoreceptor outer segment formation. *Hum Mol Genet*. 2018;27:3507–3518.
- Boon CJ, den Hollander AI, Hoyng CB, Cremers FP, Klevering BJ, Keunen JE. The spectrum of retinal dystrophies caused by mutations in the peripherin/RDS gene. *Prog Retin Eye Res*. 2008;27:213–235.
- Dryja TP, Hahn LB, Kajiwara K, Berson EL. Dominant and digenic mutations in the peripherin/RDS and ROM1 genes in retinitis pigmentosa. *Invest Ophthalmol Vis Sci*. 1997;38:1972–1982.
- Kajiwara K, Berson EL, Dryja TP. Digenic retinitis pigmentosa due to mutations at the unlinked peripherin/RDS and ROM1 loci. *Science*. 1994;264:1604–1608.
- Ma CJ, Lee W, Stong N, et al. Late-onset pattern macular dystrophy mimicking ABCA4 and PRPH2 disease is caused by a homozygous frameshift mutation in ROM1. *Cold Spring Harb Mol Case Stud*. 2019;5(3):a003624.
- Conley SM, Stuck MW, Watson JN, Naash MI. Rom1 converts Y141C-Prph2-associated pattern dystrophy to retinitis pigmentosa. *Hum Mol Genet*. 2017;26:509–518.
- Poloschek CM, Bach M, Lagreze WA, et al. ABCA4 and ROM1: implications for modification of the PRPH2-associated macular dystrophy phenotype. *Invest Ophthalmol Vis Sci*. 2010;51:4253–4265.

21. Feist RM, White MF, Jr., Skalka H, Stone EM. Choroidal neovascularization in a patient with adult foveomacular dystrophy and a mutation in the retinal degeneration slow gene (Pro 210 Arg). *Am J Ophthalmol*. 1994;118:259–260.
22. Gorin MB, Jackson KE, Ferrell RE, et al. A peripherin/retinal degeneration slow mutation (Pro-210-Arg) associated with macular and peripheral retinal degeneration. *Ophthalmology*. 1995;102:246–255.
23. Zhuk SA, Edwards AO. Peripherin/RDS and VMD2 mutations in macular dystrophies with adult-onset vitelliform lesion. *Mol Vis*. 2006;12:811–815.
24. Duncan JL, Ratnam K, Birch DG, et al. Abnormal cone structure in foveal schisis cavities in X-linked retinoschisis from mutations in exon 6 of the RS1 gene. *Invest Ophthalmol Vis Sci*. 2011;52:9614–9623.
25. Reeves MJ, Goetz KE, Guan B, et al. Genotype-phenotype associations in a large PRPH2-related retinopathy cohort. *Human Mutation*. 2020;41:1528–1539.
26. Chakraborty D, Strayve DG, Makia MS, et al. Novel molecular mechanisms for Prph2-associated pattern dystrophy. *FASEB J*. 2020;34:1211–1230.
27. Chakraborty D, Conley SM, Stuck MW, Naash MI. Differences in RDS trafficking, assembly and function in cones versus rods: insights from studies of C150S-RDS. *Hum Mol Genet*. 2010;19:4799–4812.
28. Stricker HM, Ding XQ, Quiambao AB, Naash MI. The C214S mutation in peripherin/rds confers protein instability. *Protein Science*. 2003;12:111.
29. Chakraborty D, Conley SM, Zulliger R, Naash MI. The K153Del PRPH2 mutation differentially impacts photoreceptor structure and function. *Hum Mol Genet*. 2016;25:3500–3514.
30. Stuck MW, Conley SM, Naash MI. The Y141C knockin mutation in RDS leads to complex phenotypes in the mouse. *Hum Mol Genet*. 2014;23:6260–6274.
31. Conley SM, Stuck MW, Burnett JL, et al. Insights into the mechanisms of macular degeneration associated with the R172W mutation in RDS. *Hum Mol Genet*. 2014;23:3102–3114.
32. Vingrys AJ, King-Smith PE. A quantitative scoring technique for panel tests of color vision. *Invest Ophthalmol Vis Sci*. 1988;29:50–63.
33. Bennett LD, Klein M, Locke KG, Kiser K, Birch DG. Dark-Adapted Chromatic Perimetry for Measuring Rod Visual Fields in Patients with Retinitis Pigmentosa. *Transl Vis Sci Technol*. 2017;6:15.
34. Bennett LD, Metz G, Klein M, Locke KG, Khwaja A, Birch DG. Regional Variations and Intra-/Intersession Repeatability for Scotopic Sensitivity in Normal Controls and Patients With Inherited Retinal Degenerations. *Invest Ophthalmol Vis Sci*. 2019;60:1122–1131.
35. McCulloch DL, Marmor MF, Brigell MG, et al. ISCEV Standard for full-field clinical electroretinography (2015 update). *Documenta Ophthalmologica Adv Ophthalmol*. 2015;130:1–12.
36. Birch DG, Anderson JL. Standardized full-field electroretinography. Normal values and their variation with age. *Arch Ophthalmol*. 1992;110:1571–1576.
37. Zulliger R, Conley SM, Mwoyosvi ML, Stuck MW, Azadi S, Naash MI. SNAREs Interact with Retinal Degeneration Slow and Rod Outer Segment Membrane Protein-1 during Conventional and Unconventional Outer Segment Targeting. *PLoS One*. 2015;10:e0138508.
38. Conley SM, Stricker HM, Naash MI. Biochemical analysis of phenotypic diversity associated with mutations in codon 244 of the retinal degeneration slow gene. *Biochemistry*. 2010;49:905–911.
39. Oishi A, Fujinami K, Mawatari G, et al. Genetic and Phenotypic Landscape of PRPH2-Associated Retinal Dystrophy in Japan. *Genes*. 2021;12:1817.
40. Acton JH, Bartlett NS, Greenstein VC. Comparing the Nidek MP-1 and Humphrey field analyzer in normal subjects. *Optom Vis Sci: Official Publication of the American Academy of Optometry*. 2011;88:1288–1297.
41. Haegerstrom-Portnoy G, Schneck ME, Lott LA, Hewlett SE, Brabyn JA. Longitudinal Increase in Anisometropia in Older Adults. *Optometry Vis Sci*. 2014;91:60–67.
42. Scheffrin BE. *Diagnosis of Defective Colour Vision*, by Birch J. New York, NY: Oxford University Press; 1993: Paperback, 187 pp. *Color Research & Application* 1994;19:484–484.
43. Francois J, Verriest G. [Acquired dyschromatopsia in primary glaucoma]. *Ann Ocul (Paris)*. 1959;192:191–199.
44. Drance SM, Lakowski R, Schulzer M, Douglas GR. Acquired color vision changes in glaucoma. Use of 100-hue test and Pickford anomaloscope as predictors of glaucomatous field change. *Arch Ophthalmol*. 1981;99:829–831.
45. Papaconstantinou D, Georgalas I, Kalantzis G, et al. Acquired color vision and visual field defects in patients with ocular hypertension and early glaucoma. *Clin Ophthalmol*. 2009;3:251–257.
46. Pacheco-Cutillas M, Edgar DF, Sahraie A. Acquired colour vision defects in glaucoma-their detection and clinical significance. *Br J Ophthalmol*. 1999;83:1396–1402.
47. Cheng T, Peachey NS, Li S, Goto Y, Cao Y, Naash MI. The effect of peripherin/rds haploinsufficiency on rod and cone photoreceptors. *J Neurosci*. 1997;17:8118–8128.
48. Ding XQ, Nour M, Ritter LM, Goldberg AF, Fliesler SJ, Naash MI. The R172W mutation in peripherin/rds causes a cone-rod dystrophy in transgenic mice. *Hum Mol Genet*. 2004;13:2075–2087.
49. Applebury ML, Antoch MP, Baxter LC, et al. The murine cone photoreceptor: a single cone type expresses both S and M opsins with retinal spatial patterning. *Neuron*. 2000;27:513–523.
50. Nadal-Nicolas FM, Kunze VP, Ball JM, et al. True S-cones are concentrated in the ventral mouse retina and wired for color detection in the upper visual field. *Elife*. 2020;9:e56840.
51. Sun H, Molday RS, Nathans J. Retinal stimulates ATP hydrolysis by purified and reconstituted ABCR, the photoreceptor-specific ATP-binding cassette transporter responsible for Stargardt disease. *J Biologic Chem*. 1999;274:8269–8281.
52. Farjo R, Skaggs JS, Nagel BA, et al. Retention of function without normal disc morphogenesis occurs in cone but not rod photoreceptors. *J Cell Biol*. 2006;173:59–68.
53. Kedzierski W, Nusinowitz S, Birch D, et al. Deficiency of rds/peripherin causes photoreceptor death in mouse models of digenic and dominant retinitis pigmentosa. *Proc Natl Acad Sci USA*. 2001;98:7718–7723.
54. Nour M, Ding XQ, Stricker H, Fliesler SJ, Naash MI. Modulating expression of peripherin/rds in transgenic mice: critical levels and the effect of overexpression. *Invest Ophthalmol Vis Sci*. 2004;45:2514–2521.
55. Farjo R, Fliesler SJ, Naash MI. Effect of Rds abundance on cone outer segment morphogenesis, photoreceptor gene expression, and outer limiting membrane integrity. *J Compar Neurol*. 2007;504:619–630.
56. Stricker HM, Ding XQ, Quiambao A, Fliesler SJ, Naash MI. The Cys214->Ser mutation in peripherin/rds causes a loss-of-function phenotype in transgenic mice. *Biochemical J*. 2005;388:605–613.
57. Goldberg AF, Fales LM, Hurley JB, Khattree N. Folding and subunit assembly of photoreceptor peripherin/rds is mediated by determinants within the extracellular/intradiskal EC2 domain: implications for heterogeneous molecular pathologies. *J Biologic Chem*. 2001;276:42700–42706.

58. Shankar SP, Hughbanks-Wheaton DK, Birch DG, et al. Autosomal Dominant Retinal Dystrophies Caused by a Founder Splice Site Mutation, c.828+3A>T, in PRPH2 and Protein Haplotypes in trans as Modifiers. *Invest Ophthalmol Vis Sci.* 2016;57:349–359.
59. Downes SM, Fitzke FW, Holder GE, et al. Clinical features of codon 172 RDS macular dystrophy: similar phenotype in 12 families. *Arch Ophthalmol.* 1999;117:1373–1383.
60. Wroblewski JJ, Wells JA, 3rd, Eckstein A, et al. Macular dystrophy associated with mutations at codon 172 in the human retinal degeneration slow gene. *Ophthalmology.* 1994;101:12–22.
61. Conley SM, Al-Ubaidi MR, Han Z, Naash MI. Rim formation is not a prerequisite for distribution of cone photoreceptor outer segment proteins. *FASEB J.* 2014;28:3468–3479.
62. Stuck MW, Conley SM, Naash MI. The Y141C knockin mutation in RDS leads to complex phenotypes in the mouse. *Hum Mol Genet.* 2014;23:6260–6274.